Hindawi
Advances in Civil Engineering
Volume 2024, Article ID 5542173, 10 pages
https://doi.org/10.1155/2024/5542173

Research Article

Study on the Wind Deviation Characteristics of Y-Type Insulator String under the Action of Strong Wind

Xianren Wang,[1] Chuiwei Yang,[2] Jiaqian Zhang,[2] Junyu Zhou,[1] Hangzhang Liang,[1] Jing Jiang,[1] Yonghui Cai,[1] Mojia Huang,[1] and Zhiwen Lan[1]

[1]*Institute of Engineering Mechanics, Nanchang University, 999 Xuefu Avenue, Nanchang 330031, China*
[2]*China Energy Engineering Group Anhui Electric Power Design Institute Co., Ltd., 369 Fanhua Avenue, Hefei 230601, China*

Correspondence should be addressed to Zhiwen Lan; zwlan@ncu.edu.cn

Received 22 November 2023; Revised 18 January 2024; Accepted 29 January 2024; Published 8 February 2024

Academic Editor: Hossein Nassiraei

Under the action of extreme wind load, the overhead transmission line will generate a wind deflection flashover phenomenon, which seriously affects the normal operation of the transmission system and causes significant losses. Y-type insulator string (hereinafter referred to as Y-string) is an optimized structural form to reduce the wind deflection flashover in windy areas, and the dynamic mechanical characteristics of Y-string under the action of pulsating wind is an important factor that influences the design of the overhead transmission line. The calculation method of pulsating wind load and the static calculation method of wind deflection displacement of Y-string are obtained through theoretical derivation. The mathematical software is used to simulate the time course of pulsating wind speed and convert it into the time course of wind load, establish the finite element model of insulator string, simulate and analyze the wind deflection process of Y-string under the action of pulsating wind by using the finite element method, and calculate the horizontal displacement of Y-string under the excitation of pulsating wind and make a comparative analysis with the results of the static calculations. The results show that the wind deflection displacement of the Y-string under pulsating wind is 1.12–1.28 times that under steady-state wind, which reveals the reason for the wind deflection flashover phenomenon and provides theoretical references for the design and improvement of overhead transmission lines.

1. Introduction

With the expansion of the power grid, the phenomenon of wind-induced conductor galloping and flashover in overhead transmission lines during strong wind weather has become increasingly severe [1]. Studying the wind-induced response of overhead transmission lines under strong wind conditions is of great significance for the design of transmission lines.

Currently, there has been extensive research conducted both domestically and internationally on the wind-induced response of transmission lines and insulator strings under pulsating wind. Literatures [2, 3] have established four numerical models for insulator strings and conductors, systematically studying the wind-induced characteristics of ultrahigh-voltage insulator strings under pulsating wind. It is believed that the fluctuation response coefficient of the wind deflection angle of insulator strings under different conditions is approximately 1.1–1.2. Literatures [4, 5] have established V-type ceramic insulator string and composite insulator string models, and through finite element analysis, it was found that the friction and limiting between ceramic insulators have a small impact on the overall force of the string, and the composite insulator string can still undergo significant deformation after buckling. When calculating wind deflection, the compression of the leeward insulator string should be considered. Literatures [6–8] studied the wind deflection characteristics of V-type composite insulator strings considering the backwind limb pressure. Literatures [9, 10] have established a suspension insulator string model, considering the dynamic response of insulator strings under pulsating wind, and it is believed that the dynamic characteristics of wind have a significant impact on the wind deflection of suspension insulator strings. The dynamic stiffness of overhead transmission lines and the nonlinear coupled vibrations have been studied and analyzed in the literatures [11–13]. Literatures [14–16] have established a transmission line–insulator string coupling model, conducting transient

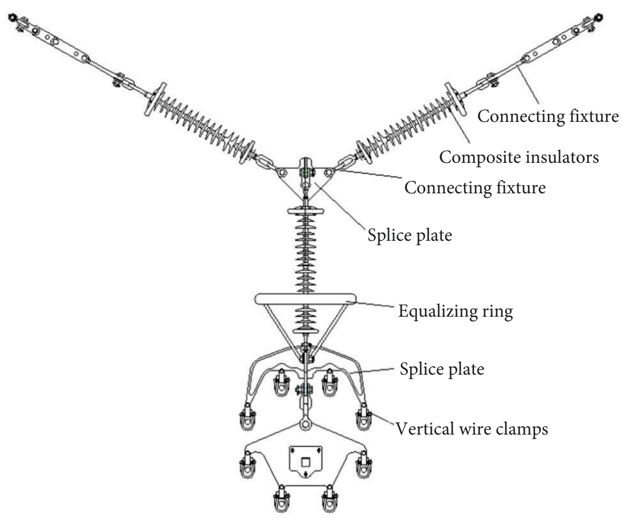

Figure 1: Y-type insulator string structure schematic diagram.

dynamic analysis under average wind, gust wind, and pulsating wind fields and comparing and analyzing the impact of different factors on insulator string wind deflection. Literatures [17, 18] have summarized the wind deflection calculation methods for foreign V-type insulator strings and studied the bearing capacity of the leeward limb of the V-string. The wind deflection and buckling characteristics of Y-shaped insulator strings under strong winds have been studied in the literatures [19, 20]. The above studies have been carried out on type I and type V insulator strings and fewer studies have been carried out on the wind deflection characteristics of Y-type insulator strings under pulsating winds. The structure of Y-type insulator strings is shown in Figure 1. Y-type insulator strings are generally used in extra-high-voltage linear towers (e.g., Figure 2), which will cause huge economic losses in the event of wind deflection and flashover accidents. Therefore, the study of wind deflection characteristics of Y-type insulator string under strong wind has certain engineering significance.

This article focuses on a four-span overhead transmission line as the research object, simulating the pulsating wind speed time history in different sections of the transmission line. The dynamic wind deviation characteristics of the Y-string under different wind speeds were systematically studied, providing a reference basis for the design of transmission line engineering.

2. Calculation of Wind Load

2.1. Calculation of Wind Load According to Current Specifications. According to the current specifications [21], the wind load on the transmission line can be calculated using the following equation:

$$W_x = \alpha \cdot W_0 \cdot \mu_z \cdot \mu_{sc} \cdot \beta_c \cdot d \cdot L_p \cdot B \cdot \sin^2\theta, \quad (1)$$

$$W_0 = {v_0}^2/1{,}600. \quad (2)$$

In the equation, W_x represents the wind load on the conductor (kN); α is the wind pressure nonuniformity factor;

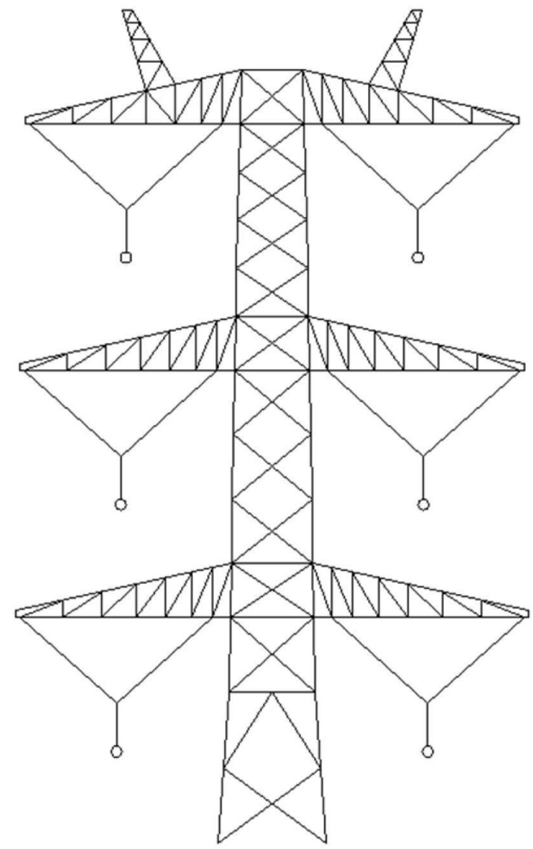

Figure 2: Y-type insulator string tower for a double-circuit transmission line.

W_0 is the reference wind pressure (kN/m^2); μ_z is the wind pressure height variation factor; β_c is the wind load adjustment factor; μ_{sc} is the conductor shape factor; d is the outer diameter of the conductor or the calculated diameter when covered with ice (m); L_p is the horizontal span between towers (m); θ is the angle between the wind direction and the conductor direction (°); v_0 is the basic wind speed at a height of 10 m (m/s).

The adjustment factor β_c introduced in the above equation considers the resonance effect of gusty winds and is proportional to the average wind speed at a height of 10 m, independent of the wind's fluctuation characteristics, which is evidently unreasonable [22]. The unreasonable choice of β_c values is one of the reasons for the frequent occurrence of wind-induced conductor galloping in recent years.

2.2. Calculation of Gusty Wind Load. The action of natural wind on conductors belongs to dynamic effects, and the calculation of wind load on conductors should take into account the dynamic amplification effect of gusty winds. For the calculation of structural wind load under gusty wind action, the equivalent wind-induced force method is generally used, which is equivalent to the inertial force in structural dynamics [23]. Figure 3 illustrates the phenomenon of conductor galloping under the action of wind load. The conductor undergoes static displacement under its own weight and average wind load, while under the action of gusty wind load, the

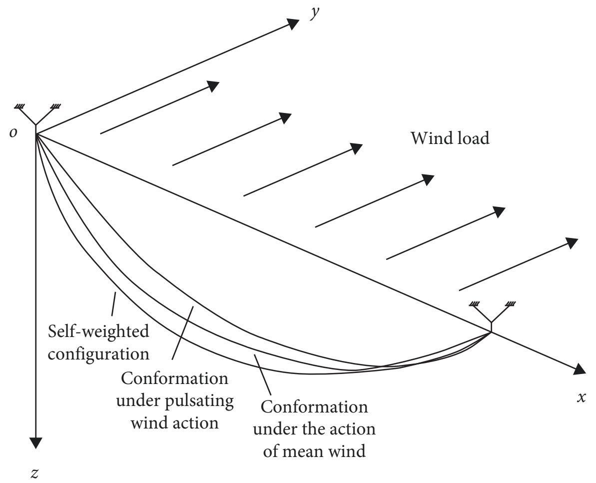

Figure 3: Schematic diagram of conductor wind deflection under wind load.

conductor oscillates back and forth near its static equilibrium position, resulting in larger displacements than under average wind load [24].

The motion equation of an infinite degree of freedom one-dimensional structure (with wind direction in the y-axis) can be written as follows:

$$M\ddot{y}_d + C\dot{y}_d + Ky_d = p(t), \tag{3}$$

where M, C, and K represent the mass, damping, and stiffness of the structure, respectively. y_d denotes the displacement of the structure in the y-direction, and $p(t)$ represents the loading function.

By employing the mode shape decomposition method for a solution, the displacement is expanded in terms of mode shapes as follows:

$$y_d(t) = \sum_{j=1}^{\infty} y_{dj}(t) = \sum_{j=1}^{\infty} \varphi_j(x) q_j(t), \tag{4}$$

where $\varphi_j(x)$ represents the value of the jth mode shape of the structure at position x, and $q_j(t)$ corresponds to the generalized coordinates of the jth mode.

Substituting $y_d(t)$ into the equation, considering the orthogonality of the mode shapes with respect to mass and stiffness, assuming proportional damping or uncoupled damping, the damping coefficient of the jth mode represented by the damping ratio ζ_1, the generalized coordinate equation can be obtained as follows:

$$\ddot{q}_j(t) + 2\zeta_1\omega_j\dot{q}_j(t) + \omega_j^2 q_j(t) = F_j(t). \tag{5}$$

Since $F_j(t)$ contains the randomness of $f(t)$, it is necessary to solve the equation using the theory of random vibrations. According to the theory of random vibrations, the root mean square of displacement response can be expressed as follows:

$$\begin{aligned}\sigma_y(x) &= \sqrt{\int_{-\infty}^{+\infty} S_y(x,\omega)d\omega} = \sqrt{\sum_{j=1}^{\infty}\sigma_{yj}^2} \\ &= \sqrt{\sum_{j=1}^{\infty}\varphi_j^2(x)\int_{-\infty}^{+\infty}|H_j(i\omega)|^2 S_{F_jF_j}(\omega)d\omega.}\end{aligned} \tag{6}$$

So

$$y_d(x) = \mu\sigma_y(x) = \left[\sum_{j=1}^{\infty}\left(\frac{\xi_j u_j \varphi_j(x) w_0}{\omega_j^2}\right)^2\right]^{\frac{1}{2}} = \left[\sum_{j=1}^{\infty} y_{dj}(x)\right]^{\frac{1}{2}}. \tag{7}$$

In terms of displacement for engineering purposes, the influence of the first mode shape plays a predominant role. Therefore, considering only the first mode, the equation can be written as follows:

$$y_d(x) \approx y_{d1}(x) = \frac{\xi_1 u_1 \varphi_1(x) w_0}{\omega_1^2}. \tag{8}$$

In the equation, ξ_j is referred to as the amplification factor of the jth mode due to gusty winds, while u_j represents the influence coefficient of the jth mode.

To determine the amplification factor ξ_1, it is necessary to have prior knowledge of the wind spectral density $S_f(\omega)$. In this study, the Davenport [25] spectrum is adopted.

$$S_v(n) = 4K\overline{v_{10}^2}\frac{x_0^2}{n(1+x_0^2)^4}, \tag{9}$$

$$x_0 = \frac{1,200n}{\overline{v_{10}}.} \tag{10}$$

By substituting the equation into the conversion formula between the wind speed spectrum and the wind pressure spectrum, we obtain the following:

$$S_\omega(x,z,n) = 16K\overline{\omega}^2\frac{\overline{v}_{10}^2}{\overline{v}^2}\frac{x_0^2}{n(1+x_0^2)^{\frac{4}{3}}}, \tag{11}$$

$$\begin{aligned}\xi_1 &= \omega_1^2\sqrt{\int_{-\infty}^{+\infty}|H_j(i\omega)|^2 S_f(\omega)d\omega} = \sqrt{1 + S_f(n_1)\cdot\frac{\pi\zeta_1 n_1}{(2\zeta_1)^2}} \\ &= \sqrt{1 + \frac{x_1^2\frac{\pi}{6\zeta_1}}{(1+x_1^2)^{4/3}}},\end{aligned} \tag{12}$$

$$x_1 = \frac{30}{\sqrt{W_0 T_1^2}}. \tag{13}$$

Based on structural dynamics, assuming the mode shape function as a sine function $\varphi_1(x) = \sin\frac{\pi x}{l}$, the calculation expression for the wind-induced vibration coefficient is as follows:

Table 1: Wind load calculation results under different calculation methods.

Wind speed (m/s)	Static results (N)	Dynamic results (N)	λ
15	5,575.9	6,632.8	1.19
20	9,268.4	12,082.5	1.30
25	15,798.3	19,247.0	1.22
30	20,073.2	28,216.0	1.40

Note: λ Represents the ratio between the dynamic calculation results and the static calculation results of wind load on the transmission line.

$$\beta_c = \left(1 + \frac{4}{\pi}\xi_1\mu_f\eta_{x1}\varphi_1(x)\right)\left(\frac{H}{10}\right)^{-2\alpha}. \tag{14}$$

The calculation formula for gusty wind load on transmission lines is as follows:

$$P_H = \beta_c\mu_s\mu_z W_0 dL_p. \tag{15}$$

Case: Considering a horizontal span of 400 m and an average height of the conductor above the ground of 20 m, with the transmission line passing through a Class C terrain. The conductor model is JL3/G1A-400/35 ACSR (aluminum conductor steel reinforced), and the normal operating tension of the conductor is 19,703 N. Comparison of wind loads on transmission lines at different wind speeds calculated by the above two wind load calculation methods is shown in Table 1.

From Table 1, it can be observed that the wind load calculation results for dynamic transmission line analysis considering gusty wind effects are 1.19–1.40 times higher than the wind load calculation results based on the current specifications for different wind speeds. The ratio between the dynamic and static results of wind load on the transmission line increases as the wind speed becomes higher.

3. Theoretical Calculation of Static Wind Deviation for Y-String Insulator Assembly

3.1. Theoretical Calculation of Wind Deviation for Y-String Assembly. Currently, when calculating the wind deviation of insulator assemblies, the assembly is often simplified as a rigid body, and the forces acting on it under wind load are calculated based on the principles of static equilibrium [26]. For the Y string, the wind deflection calculation is schematically shown in Figure 4.

The forces acting on the Y-string insulator assembly primarily include the wind load on the conductor P_H and the self-weight of the conductor G_V. According to the principles of static equilibrium, the resultant force of the external load F, the force acting on the windward limb F_1, the force acting on the leeward limb F_2, and the wind deviation angle φ_n are given by the following:

$$F = \sqrt{P_H^2 + G_V^2}, \tag{16}$$

$$F_1 = \frac{\sin(\varphi_n + \theta/2)}{\sin\theta}F, \tag{17}$$

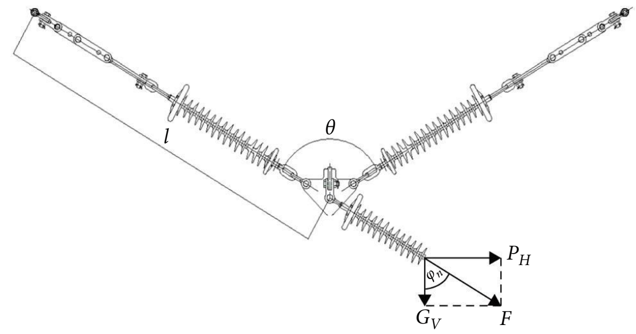

Figure 4: Schematic diagram of Y-string wind deflection rigid body static force method.

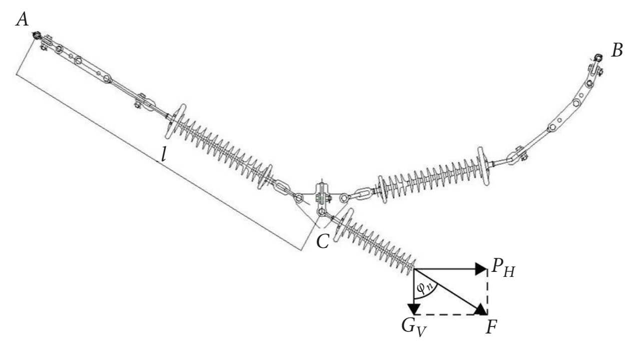

Figure 5: Schematic diagram of Y-string wind deflection.

$$F_2 = \frac{\sin(\theta/2 - \varphi_n)}{\sin\theta}F, \tag{18}$$

$$\varphi_n = a\tan\frac{P_H}{G_V}. \tag{19}$$

In the equation, φ_n represents the wind deviation angle of the insulator assembly, θ represents the included angle of the insulator assembly. From the equation, it can be observed that when $\theta/2>\varphi_n$, both F_1 and F_2 are greater than zero, indicating that both sides of the insulator assembly are under tension. When $\theta/2=\varphi_n$, $F_1=F$ and $F_2=0$, indicating that the windward limb bears the entire external force while the leeward limb remains unloaded. When $\theta/2<\varphi_n$, $F_1>0$ and $F_2<0$, indicating that the leeward limb is under compression. However, to prevent the insulator assembly from being compressed and relaxed, some literature specifies that the insulator assembly should not be subjected to compression. Some researchers argue that the leeward limb of the insulator assembly can withstand certain levels of compression, especially when composite insulator assemblies exhibit stable flexural deformation capabilities [1]. Therefore, when the leeward limb of the insulator assembly is subjected to compression, the above equation is no longer applicable. When the insulator string is under pressure, the wind deflection is schematically shown in Figure 5.

Assuming the coordinate origin is point A, and the length of the insulator assembly is denoted as l, the trajectory of point C's motion is as follows:

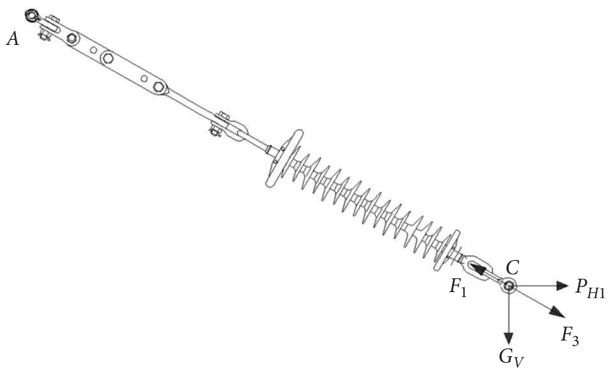

Figure 6: Stress analysis diagram of a tensile limb.

$$x_C^2 + y_C^2 = l^2. \quad (20)$$

By geometric relationship, we can derive the following equation:

$$\overline{BC} = \sqrt{l^2 + 4l^2 sin^2\frac{\theta}{2} - 4lsin\frac{\theta}{2}x_c}. \quad (21)$$

For the tensile limb point C, the analysis is shown in Figure 6.

$$P_{H1} = G_V \tan\varphi_n. \quad (22)$$

Let the axial deformation of the limb under compression be denoted as Δl, then we have the following:

$$\overline{BC} + \Delta l = l. \quad (23)$$

By solving the above equations simultaneously, we obtain the following:

$$x_C = \frac{4l^2\sin^2\frac{\theta}{2} - \Delta l^2 + 2l\Delta l}{4l\sin\frac{\theta}{2}}, \quad (24)$$

where P_{H1} represents the horizontal wind load component on the windward limb, F_1 represents the tension force on the windward limb, and F_3 represents the force exerted by the windward limb on the leeward limb.

The analysis for the compressed limb point C is shown in Figure 7.

By the geometric similarity relationship, we can obtain the following equation:

$$\frac{P_{H2}}{\overline{AB}} = \frac{F_2}{\overline{BC}}. \quad (25)$$

That is to say:

$$P_{H2} = \frac{2l\sin\frac{\theta}{2}}{\sqrt{l^2 + 4l^2\sin^2\frac{\theta}{2} - 4l\sin\frac{\theta}{2}x_c}}, \quad (26)$$

where P_{H2} represents the horizontal wind load component on the leeward limb, and F_2 represents the pressure exerted on the leeward limb.

The pressure F_2 on the leeward limb is related to its axial displacement Δl and can be obtained through a buckling analysis considering large deflection. By using the above equations, the axial displacement of the leeward limb and the force distribution between the two limbs can be determined under different horizontal wind loads.

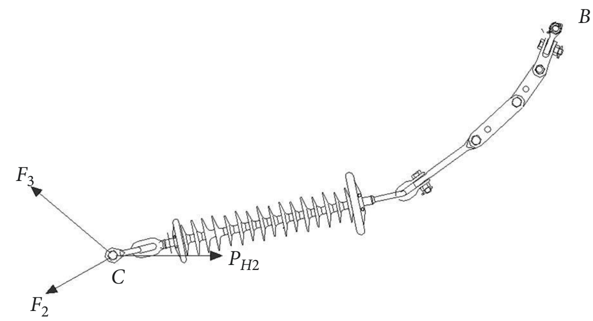

Figure 7: Stress analysis diagram of compression limb.

Table 2: Parameters of FXBW-500/210-2 composite insulator.

Symbol	Quantity
Elastic modulus E (MPa)	40,000
Poisson's ratio (μ)	0.3
Rod core diameter (mm)	48
Nominal structure height (mm)	4,450
Rated mechanical tensile load (KN)	210

3.2. Finite Element Analysis of Buckling in the Compressed Limb. Considering a Y-string with a limb angle of 90°, an I-section length of 1 m, and limb lengths of 6 m, as shown in the diagram below. The Y-string suspends a conductor of type JL3/G1A-400/35, with a conductor self-weight of 26,980 N. The parameters of the Y-string are listed in Table 2. Finite element simulation of the buckling in the compressed limb of the Y-string is conducted, as shown in Table 2.

Based on the connection method of composite insulators, one end is hinged, and the other end is sliding. The calculation formula for the critical buckling force P_{cr} of the composite core rod experiencing compressive buckling instability is as follows:

$$P_{cr} = \frac{\pi^2 EI}{(\mu l)^2} = \frac{\pi^2 \times 40 \times 10^9 \times \frac{\pi \times 0.048^4}{64}}{(1 \times 6)^2} = 2{,}857.5\ \text{N}. \quad (27)$$

The buckling analysis of the compressed limbs of the Y-string was performed using finite element software to obtain the first five mode shapes. The first mode buckling load was calculated as 2,861.9 N, which is in good agreement with the theoretical calculation results. Based on the eigenvalue buckling analysis, a nonlinear buckling analysis was conducted on the composite core rod to study the stress and deformation characteristics after buckling of the compressed limbs. The relationship between axial displacement and axial force is shown in Figure 8.

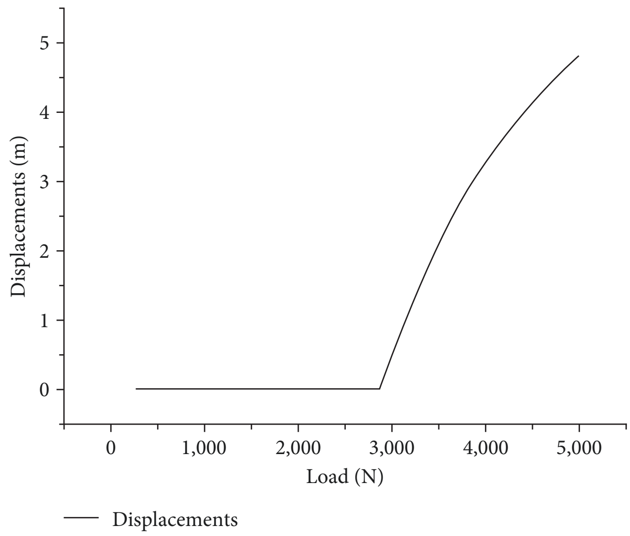

Figure 8: Change law of axial displacement and axial force.

According to Figure 8, the compressed limbs remain stable before reaching the critical load of 2,861.9 N without experiencing buckling instability. As the load increases, the core rod still possesses a certain load-bearing capacity even after buckling instability occurs.

4. Y-Type Insulator String Wind Deviation Finite Element Simulation

4.1. Wind Load Time History Simulation. The fluctuating wind load is a random load and represents the dynamic component of the wind load. Under the action of fluctuating wind, structures experience random vibrations. Before analyzing the structural response to fluctuating wind, it is necessary to determine the probability distribution and power spectral density of the fluctuating wind. Existing research and extensive measurement data indicate that fluctuating wind speed can be considered as a zero-mean Gaussian stationary random process, meaning its statistical characteristics do not vary with the selected time period, and the wind speed spectrum follows a normal distribution [27].

Currently, researchers from various countries have proposed numerous fluctuating wind power spectra. Based on over 90 strong wind records obtained from different locations and heights worldwide, Davenport observed that the turbulent scale remains constant with height in the fluctuating wind velocity spectrum. Consequently, Davenport proposed the well-known Davenport spectrum:

$$S_u(n) = 4K\overline{v}_{10}^2 \frac{x^2}{n(1+x^2)^{\frac{4}{3}}}, \tag{28}$$

$$x = \frac{1,200n}{\overline{v}_{10}}, \tag{29}$$

where n is the frequency of the wind (Hz), $\overline{v}_{10}$ is the mean wind speed at a height of 10 m (m/s), and K is a coefficient related to the ground roughness.

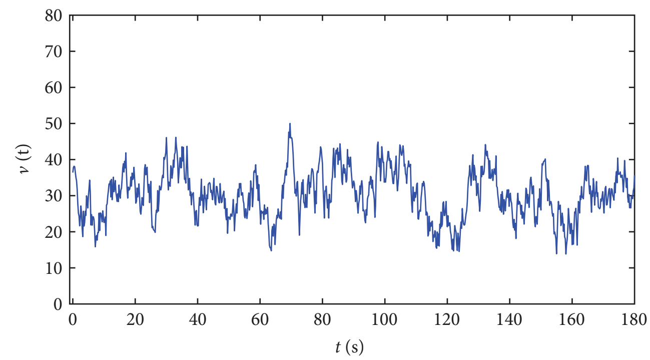

Figure 9: Pulsating wind time history diagram.

Some researchers argue that the turbulent scale decreases with increasing height. Therefore, Davenport assumed that the turbulent scale remains constant with height for conservative considerations. In 1972, Kaimal proposed the Kaimal spectrum, which accounts for the variation of turbulent scale with height as follows:

$$S_u(z,n) = 105u_*^2 \frac{f}{n(1+33f)^{\frac{5}{3}}}, \tag{30}$$

$$u_* = \frac{0.4\overline{v}_z}{\ln\left(\frac{z}{z_0}\right)}. \tag{31}$$

The commonly used Kaimal spectrum in engineering was revised by Simiu in 1974 and became known as the Simiu spectrum as follows:

$$S_u(z,n) = 200u_*^2 \frac{f}{n(1+50f)^{\frac{5}{3}}}, \tag{32}$$

where u_* is the friction velocity, v_z is the average wind speed at height z, z_0 is the ground roughness length, and $\overline{v}_{10}$ is the dimensionless number.

As described above, mathematical modeling software can be used to simulate wind speed spectra. Assuming a terrain category of class C, $\overline{v}_{10} = 25$ m/s, $K = 0.00464$, average height above ground is 50 m, with $N = 500$ frequency divisions and a cutoff frequency of $\omega = 8\pi$ rad/s. The wind speed time scale and spectrum are obtained, as shown in Figures 9 and 10.

Based on the quasi-steady assumption [28], the formula for calculating the time history of fluctuating wind load is as follows:

$$W_x = \frac{1}{2}\rho C_D A v^2. \tag{33}$$

The equation includes ρ for air density and C_D for the drag coefficient of the conductor.

The wind load timescale obtained from the above equation is shown in Figure 11.

4.2. Y-String Wind Deviation Finite Element Simulation. In this section, a continuous four-span transmission line-insulator

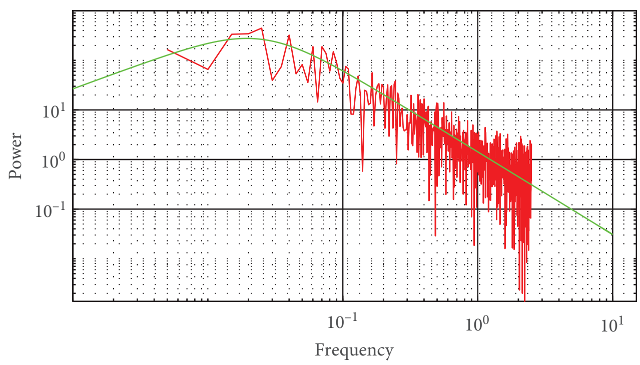

Figure 10: Pulsating wind power spectrum.

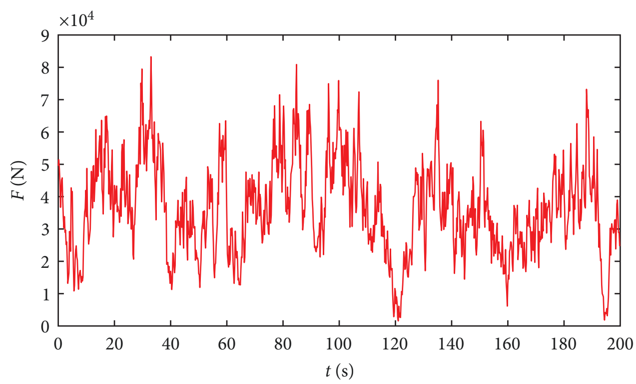

Figure 11: Time history diagram of fluctuating wind load.

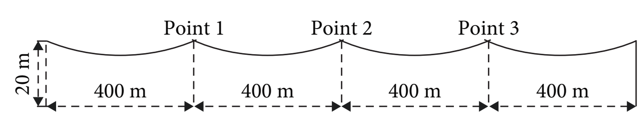

Figure 12: Schematic diagram of a continuous four-span transmission line.

string coupling model (Figure 12) is developed using the finite element method to calculate the wind deflection characteristics of the Y-type insulator string under pulsating wind load. The selected conductor model is JL3/G1A-400/35, with a span of 400 m. The insulator string chosen is the FXPW-1000/300 composite insulator string, with an I-section length of 2 m and two limb lengths of 9 m. The angle of the V segment is 120° (Figure 13). The basic parameters are summarized in Tables 3 and 4. Considering the computer performance and computational efficiency, the influence of the transmission tower is not considered in the finite element analysis, and the connection between the insulator string and the tower is regarded as a fixed articulated connection in the establishment of the finite element model. When wind deflection occurs in the conductor, the two limbs of the insulator string mainly bear the tensile force, but when the wind deflection angle is too large, the backwind limb of the composite insulator string will bear a certain pressure and buckling may occur, so the finite element simulation uses beam unit, beam189 unit compared to

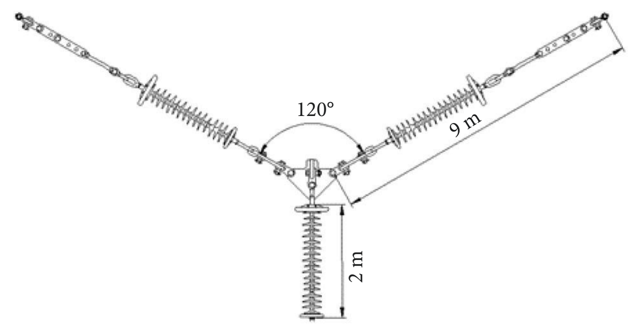

Figure 13: Depicts a schematic diagram of the Y-string insulator.

Table 3: JL3/G1A-400/35 conductor parameters.

Symbol	Quantity
Conductor diameter d (mm)	26.82
Cross-sectional area A (mm^2)	565
Elastic modulus E (MPa)	65,000
Linear mass density M (kg/m)	1.349
Rated tensile strength F (KN)	103.67

Table 4: Parameters of FXPW-1000/300 composite insulator.

Symbol	Quantity
Elastic modulus E (MPa)	40,000
Poisson's ratio (μ)	0.3
Mass per unit area (kg)	13
Height of a single piece (m)	0.195
Frontal area of a single piece (m^2)	0.03

beam44 and beam4 unit in the constraints on the constraints of the warping constraints, and beam189 can be a better definition of the material's cross-section characteristics, so the insulator string is simulated using beam189 unit. The transmission conductor has significant nonlinear characteristics and can only withstand tension but not pressure, so it is simulated by the link10 unit. Under the action of wind load, each subconductor in the bundle conductor will occur to some extent of asynchronous motion, but the overall motion is dominant, so the bundle conductor can be equated to a single conductor [29, 30].

The geometric shape of the transmission line in the static equilibrium state can be described by the hanging chain line equation, but the hanging link line equation is more complicated. In order to facilitate the calculation, when the ratio of the arc droop to the stall distance in the span is less than 0.1, the shape of the transmission line can be approximated as a parabolic shape, and the positional gap with the actual situation is very small [31]. The expression is as follows:

$$y = \frac{4f \cdot x(L - x)}{L^2} + \frac{C}{L}x, \tag{34}$$

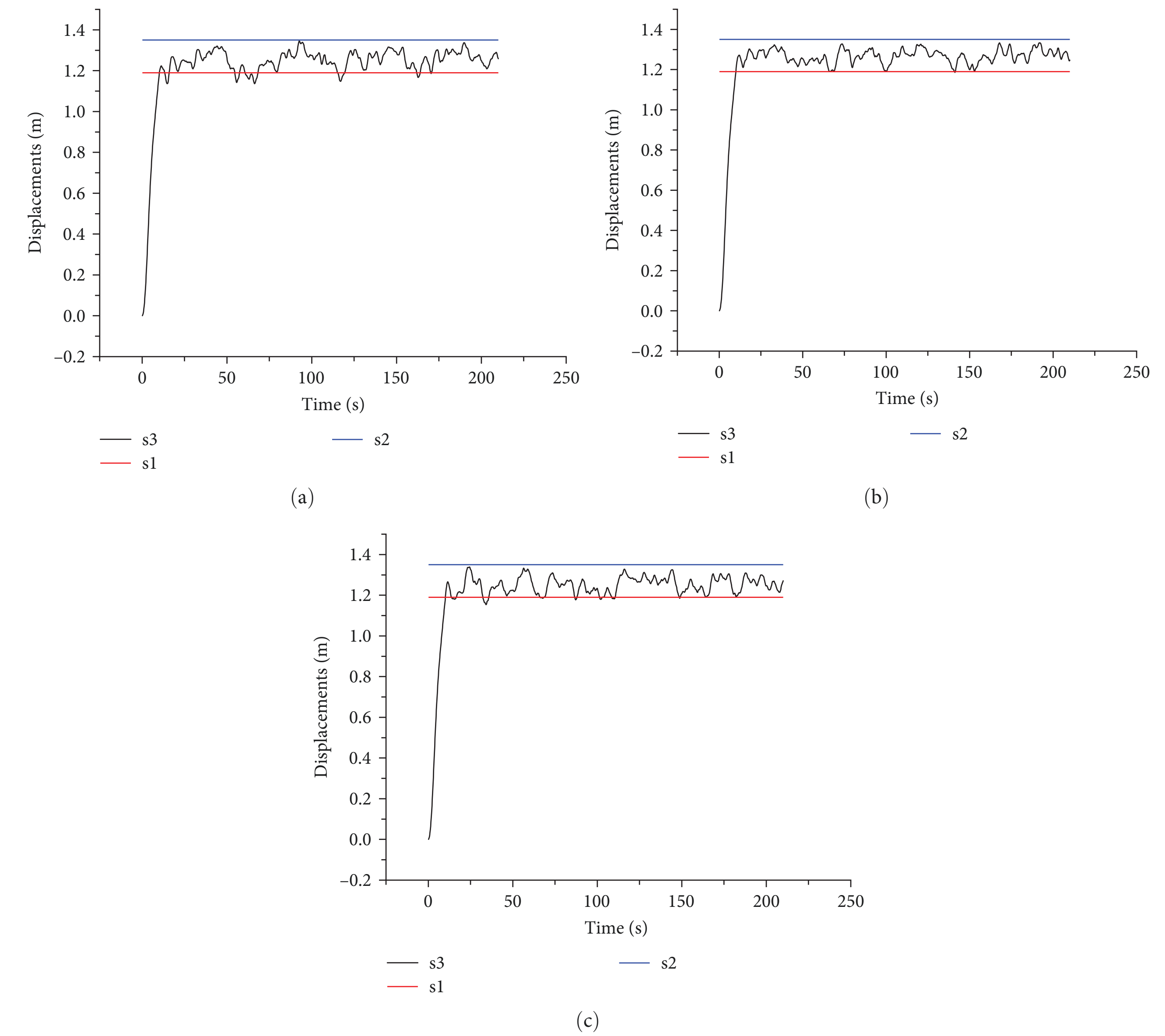

Figure 14: Wind deflection horizontal displacement history of three suspension points at 25 m/s wind speed: (a) point 1; (b) point 2; (c) point 3.

$$f = \frac{qL^2}{8T}. \tag{35}$$

The equation is defined as follows: y represents the sag at the calculation point, f is the sag at the midpoint, x is the distance from the calculation point to the suspension point, L is the span length, q is the linear mass density, C is the height difference at the suspension point, and T is the tension in the conductor.

By employing the above equation, a coupled model of the transmission line and insulator string is established, and gravitational loads are applied to analyze the conductor sag. When the transmission line is subjected to wind loads, significant displacements occur, necessitating the consideration of geometric nonlinearity. Therefore, large deformation and stress stiffening effects are considered in finite element analysis to account for the influence of geometric nonlinearity.

To prevent sudden amplification effects caused by wind loading, a linearly increasing wind load, starting from zero and reaching the average wind speed, is applied prior to the wind load time history. The fluctuating wind load is then applied to the transmission line, resulting in horizontal displacement time history at each suspension point. The time course of horizontal displacements of a hanging point at a wind speed of 25 m/s is shown in Figure 14.

The comparison between the finite element simulation results and the theoretical values for the wind-induced deflection of the Y-string insulator under fluctuating wind loads is presented in Tables 5–7.

From the above Tables 5, 6, and 7, it can be observed that under the same wind speed, the dynamic results for the Y-string

Table 5: Comparison of finite element wind deflection displacement and theoretical value of suspension point under different wind speeds.

v (m/s)	s1	s2	s3	ξ_1	ξ_2
15	0.51	0.60	0.64	1.18	1.25
20	0.80	0.99	1.02	1.24	1.28
25	1.19	1.35	1.34	1.13	1.13
30	1.38	1.60	1.58	1.16	1.14

Table 6: Comparison between finite element wind deflection displacement and theoretical value of suspension point 2 under different wind speeds.

v (m/s)	s1	s2	s3	ξ_1	ξ_2
15	0.51	0.60	0.62	1.18	1.22
20	0.80	0.99	1.00	1.24	1.25
25	1.19	1.35	1.33	1.13	1.12
30	1.38	1.60	1.57	1.16	1.14

Table 7: Comparison between finite element wind deflection displacement and theoretical value of suspension point 3 under different wind speeds.

v (m/s)	s1	s2	s3	ξ_1	ξ_2
15	0.51	0.60	0.63	1.18	1.24
20	0.80	0.99	1.00	1.24	1.25
25	1.19	1.35	1.34	1.13	1.13
30	1.38	1.60	1.58	1.16	1.14

Note: s1 represents the static calculation result of wind deflection displacement of Y-type insulator string, s2 represents the dynamic calculation result of wind deflection displacement of Y-type insulator string, s3 represents the maximum value of wind deflection displacement finite element calculation result of Y type insulator string, ξ_1 represents the ratio of s2–s1, ξ_2 represents the ratio of s3–s1.

deflection are 1.13–1.24 times larger than the static results, and the finite element simulation results are 1.12–1.28 times larger than the static results. As the wind speed increases, the ratio of dynamic results and finite element simulation results to static results decreases. Insufficient consideration of fluctuation effects in current specifications is one of the reasons for the frequent occurrence of wind-induced flashovers in recent years.

5. Conclusion

In this paper, the wind deflection displacement of Y-type insulator string under pulsating wind is calculated by theoretical analysis and finite element numerical simulation, and the static and dynamic results are compared and analyzed, and the following conclusions are drawn:

(1) The wind load under turbulent conditions is 1.19–1.40 times higher than that calculated by current standards for different wind speeds. The ratio between the two increases as the wind speed increases, indicating the need to consider the amplification effect of turbulent wind in wind load calculations.

(2) The wind-induced displacements at the attachment points of the Y-string, considering the effects of turbulence, are 1.13–1.24 times greater than those calculated by current standards for different wind speeds. The ratio between the two decreases as the wind speed increases, suggesting that the current standards inadequately account for the pulsating effects of turbulent wind.

(3) The ratio between the wind-induced displacements obtained from finite element simulations and the static calculations is 1.12–1.28. The ratio decreases with increasing wind speed. The failure of the current standards to consider the amplification effect of turbulent wind in wind load calculations contributes to the occurrence of frequent wind-induced flashover incidents.

In this paper, the wind displacement of Y-type insulator string under pulsating wind load is calculated by theoretical calculation and finite element numerical simulation. The results show that the current specification is not enough to consider the pulsating effect of wind load, and the pulsating response coefficient of wind displacement of Y-type insulator string is 1.12–1.28 under different conditions, which provides a reference basis for the design of Y-type insulator string.

Data Availability

The data used to support the findings of this study are available from the corresponding author upon request.

Conflicts of Interest

The authors declare that they have no conflicts of interest.

Acknowledgments

This research was funded by the National Natural Science Foundation of China (award no. 51568046).

References

[1] L. Zhongbin, B. Hang, Y. Xiaohui, and L. Wenjuan, "Analysis of one UHVAC transmission line windage yaw," *High Voltage Apparatus*, vol. 55, no. 1, pp. 170–177, 2019.

[2] M. Xuan, W. Zhike, Z. Yunfei, and F. Jing, "Characteristics of windage yaw in UHV insulator strings under fluctuating wind," *Electric Power*, vol. 49, no. 3, pp. 65–71, 2016.

[3] X. Xianzhong, S. Weicheng, P. Jian, and L. Hao, "Modeling and analysis of nonlinear coupled vibration of transmission line system," *Journal of Disaster Prevention and Mitigation Engineering*, vol. 36, no. 6, pp. 972–977, 2016.

[4] C. Zhou, R. J. Qin, and X. M. Rui, "Analysis of mechanical properties of V-shaped insulator string under wind load," *Chinese Journal of Engineering Design*, vol. 28, no. 1, pp. 95–104, 2021.

[5] D. Huixue, Z. Junhai, and W. Jing, "Characteristic study for windage yaw analysis of V-shape composite insulator string," *Electric Power*, vol. 49, no. 7, pp. 9–14, 2016.

[6] W. Liming, H. Ting, C. Lu, F. Kaiwei, Z. Fuzeng, and H. Zilan, "Buckling performance of polymer insulator V-type strings for 500 kV compact transmission line under gale circumstance," *High Voltage Engineering*, vol. 45, no. 4, pp. 1201–1209, 2019.

[7] L. Li, C. Lin, and X. Wu, "Research on windage yaw of V-type composite insulators in ultra-high voltage," in *2nd International Conference on Mechanics, Materials and Structural Engineering (ICMMSE)*, pp. 1–7, 2017.

[8] X. Yachao, L. Li, and Z. Xianghua, "The windage yaw force derivation of V-shaped composite insulator string based on post buckling analysis," *Engineering Journal of Wuhan University*, vol. 55, no. 8, pp. 793–798, 2022.

[9] B. Yan, X. Lin, W. Luo, Z. Chen, and Z. Liu, "Numerical study on dynamic swing of suspension insulator string in overhead transmission line under wind load," *IEEE Transactions on Power Delivery*, vol. 25, no. 1, pp. 248–259, 2010.

[10] Z. Jiayan, Y. Bo, L. Xiaohui, C. Zhida, and L. Zhongquan, "Numerical simulation of dynamic response of suspension insulator string," *Journal of Chongqing University*, vol. 29, no. 12, pp. 100–103,115, 2006.

[11] X. Hu, Z. Wang, and W. Yang, "Multi-rigid-body model of dynamic wind-induced deflection for overhead transmission lines," *Journal of Central South University of Science and Technology*, vol. 51, no. 12, pp. 3465–3474, 2020.

[12] L. Zhongbin, Z. Bo, L. Xiaohui et al., "Calculation method for dynamic stiffness of multispan overhead transmission lines," *IEEE Access*, vol. 10, pp. 64989–64999, 2022.

[13] C. Liu and M. Hou, "Wind deflection response characteristics of transmission lines under downburst," *Journal of Vibration and Shock*, vol. 41, no. 22, pp. 60–69, 2022.

[14] X. Liu, R. Huang, C. Jiang, Y. Xu, C. Li, and C. Wu, "Numerical investigation on the dynamic response and fatigue analysis of the tension insulator string under stochastic wind," *IEEE Transactions on Power Delivery*, vol. 37, no. 6, pp. 4657–4667, 2022.

[15] X. Min, G. W. Shao, Y. Z. Liu, Z. K. Wen, Y. Chen, and J. Hu, "The influence of transmission line arrangements on the swing angle of suspension insulator string," *Electric Power*, vol. 46, no. 1, pp. 69–74, 2013.

[16] H. Xin, W. Zhangqi, and T. Rui, "Sensitivity characteristics of dynamic wind-induced deflection response of insulator string on overhead lines," *Journal of Vibration Engineering*, vol. 35, no. 1, pp. 131–139, 2022.

[17] D. M. Boddy, "V-string swing angle derivation, design considerations, and structure design impacts," in *Electrical Transmission and Substation Structures Conference 2012*, 2012.

[18] Z. Zhu, J. Zhang, and X. Li, "Force analysis of V-type insulator string on compact linear tower," in *International Conference on Frontiers of Energy, Environmental Materials and Civil Engineering (FEEMCE*, pp. 722–728, 2013.

[19] B. Liu, C. Liu, K. Zhu, and S. Liu, "A study on swing and buckling of Y-type insulator strings under strong wind action for +/- 800kV UHDV transmission lines," in *2013 IEEE PES Asia-Pacific Power and Energy Engineering Conference (APPEEC)*, Hong Kong, Peoples R China, 2013.

[20] H. Bao, L. Xia, S. Chai, Y. Cheng, S. Cao, and Z. Lan, "Nonlinear buckling analysis and optimization design of the Y-type composite insulator string," *Advances in Civil Engineering*, vol. 2022, Article ID 4398388, 15 pages, 2022.

[21] Ministry of Housing and Urban-Rural Development of the People's Republic of China, *110 kV 750 kV Overhead Transmission Line Design Specification: GB 50545-2010*, China Planning Press, Beijing, 2010.

[22] Y. Bo, L. Xuesong, L. Wei, L. Zhongquan, and C. Zhida, "Research on dynamic wind load factors for windage yaw angle of suspension insulator strings," *Engineering Mechanics*, vol. 27, no. 1, pp. 221–227, 2010.

[23] Z. Xiangting, *Handbook of Wind Load Theory and Wind Resistance Calculation for Engineering Structures*, pp. 92–105, Tongji University Press, 1990.

[24] H. Xin, W. Zhangqi, and T. Rui, "Dynamic wind-induced deflection response characteristics of insulator string under slope wind attack angle," *High Voltage Engineering*, vol. 48, no. 1, pp. 289–297, 2022.

[25] A. G. Davenport, "Buffeting of a suspension bridge by storm winds," *Journal of Structural Engineering, ASCE*, vol. 8, no. 3, pp. 233–269, 1962.

[26] R. Zhou, W. Gao, and D. Zhao, "Improved calculation model for swing angle of suspension insulator string," *IET Generation, Transmission & Distribution*, vol. 11, no. 14, pp. 3644–3653, 2017.

[27] E. Simiu and R. H. Scanlan, *Wind Effects on Structures*, New York, 1996.

[28] L. Li, X. Linhai, L. Xianguo, and M. Xuan, "Windage yaw calculation method of UHV insulator strings," *High Voltage Engineering*, vol. 39, no. 12, pp. 2924–2932, 2013.

[29] X. Lin, B. Yan, Z. Liu, and Z. Chen, "Finite element simulation for windage yaw of 220kV overhead transmission lines," *Chinese Journal of Applied Mechanics*, vol. 26, no. 1, pp. 120–124, 2009.

[30] D. Stengel and M. Mehdianpour, "Finite element modelling of electrical overhead line cables under turbulent wind load," *Journal of Structures*, 2014.

[31] S. Zhenmao, *Research on Transmission Line Dance Analysis and Anti-Dance Technology*, Zhejiang University, 2010.